

FULL PAPERSubmitted to *Magnetic Resonance in Medicine*

Introduction to a novel T_2 relaxation analysis method SAME-ECOS: Spectrum Analysis for Multiple Exponentials via Experimental Condition Oriented Simulation

Hanwen Liu^{1,2*} | Qing-San Xiang^{1,3} | Roger Tam^{3,4} |
Piotr Kozlowski³ | David K.B. Li³ | Alex L. MacKay^{1,3}
| John K. Kramer^{2,5} | Cornelia Laule^{1,2,3,6}

¹Physics & Astronomy, University of British Columbia

²International Collaboration on Repair Discoveries

³Radiology, University of British Columbia

⁴Biomedical Engineering, University of British Columbia

⁵Kinesiology, University of British Columbia

⁶Pathology, University of British Columbia

Correspondence

818 W 10th Ave, Vancouver, BC, V5Z1M9
Email: hanwen@phas.ubc.ca

Present address

*818 W 10th Ave, Vancouver, BC, V5Z1M9

Funding information

Funding support was provided by the Multiple Sclerosis Society of Canada, Natural Sciences and Engineering Research Council Discovery Grant.

We propose a novel T_2 relaxation data analysis method which we have named spectrum analysis for multiple exponentials via experimental condition oriented simulation (SAME-ECOS). SAME-ECOS, which was developed based on a combination of information theory and machine learning neural network algorithms, is tailored for different MR experimental conditions, decomposing multi-exponential decay data into T_2 spectra, which had been considered an ill-posed problem using conventional fitting algorithms, including the commonly used non-negative least squares (NNLS) method. Our results demonstrated that, compared with NNLS, the simulation-derived SAME-ECOS model yields much more reliable T_2 spectra in a dramatically shorter time, increasing the feasibility of multi-component T_2 decay analysis in clinical settings.

KEYWORDS

SAME-ECOS, T_2 relaxation, non-negative least squares, resolution limit, myelin water imaging, machine learning

1 | INTRODUCTION

T_2 relaxation in biological tissues measured with a multi-echo experiment is typically characterized by multi-exponential decays because multiple water pools may exist within a single image voxel. [1] The T_2 times of different water pools are governed by the microenvironment of water molecules. For example, myelin water, the water trapped in myelin bilayers, exhibits a shorter T_2 relaxation time than that of intra/extra-cellular water (IE) and free water. [2] However, accurately depicting the spectrum of constituent T_2 components for each image voxel from MR relaxation data is nontrivial. Because the decay process of multiple water pools takes place simultaneously, the MR receiver coil can only record a signal that is the sum of multiple exponential decay components. Consequently, one has to solve a mathematical problem of fitting a superimposed relaxation signal into its constituent components. This mathematically complex problem is commonly seen in many other quantitative sciences and is often considered as an ill-posed problem. [3] The analytical and numerical solutions to this problem have been comprehensively reviewed by Istratov et al. from a mathematical perspective. [3]

To provide a suitable solution specific to MR data, Whittall and Mackay [4] introduced the non-negative least squares (NNLS) [5, 6, 7] method that decomposes the multi-echo decay data into a spectrum of positive T_2 times. The NNLS method makes no prior assumptions about the total number of T_2 components, which is a desirable feature for modeling complex biological tissues with heterogeneous compositions. However, without constraining the number of components, the T_2 fitting problem becomes underdetermined with non-unique solutions, making NNLS unstable and highly susceptible to noise even with strong regularization. In contrast, other fitting methods such as the quasi-Newton algorithm by Du et al. [8] and the Wald distribution by Akhondi-Asl et al. [9] usually provide more stable results and better noise resistance, but at the expense of modelling only two or three water pools, which limits their usage on unknown pathological tissues.

Simultaneously increasing the complexity and stability of a model is a paradox, seemingly impossible to improve one without diminishing the other in the game of multi-exponential decomposition. Our quest now was to find the line of best balance between these two factors. According to studies of information theory, the decay components can only be resolved to a certain resolution limit at a given signal to noise ratio (SNR). [10, 11] That is to say, due to noise contamination, there is always a limit in how closely the two neighboring components can be resolved, regardless of how sophisticated the analysis method is. This fundamental restriction on the resolution limit leads to a correlation between the SNR and the maximum number of components that can be reliably resolved in a particular analysis range. [12] The exact expression of this correlation is presented in the Methods, and plays a crucial role in our proposed approach.

On the other hand, machine learning algorithms, in particular supervised neural network methods [13], have been successfully implemented in many MR applications [14], especially for tasks involving parameter estimation. [15, 16] In short, a neural network can be trained to discover hidden patterns in data and to learn the mapping between two vector spaces. A trained neural network usually outperforms most conventional methods in terms of better accuracy and faster speed, particularly if the mapping is highly nonlinear. Additional background on the approximation properties of neural networks can be found elsewhere. [17]

Based on information theory and neural network algorithm approaches, we propose a novel method which we have called **Spectrum Analysis for Multi-Exponentials via Experimental Condition Oriented Simulation (SAME-ECOS)** for the analysis of multi-echo T_2 relaxation data. The general concept of SAME-ECOS (**Figure 1**) can be briefly described by a series of calculation, simulation and model training operations: (1) determine the T_2 range and resolution limit based on the experimental conditions such as SNR and echo times; (2) generate sufficient examples of random T_2 spectra within the T_2 range obeying the resolution limit; (3) compute multi-echo decay data using the randomly generated T_2 spectra; (4) train a neural network model to learn the mapping between the simulated multi-echo decay data and the

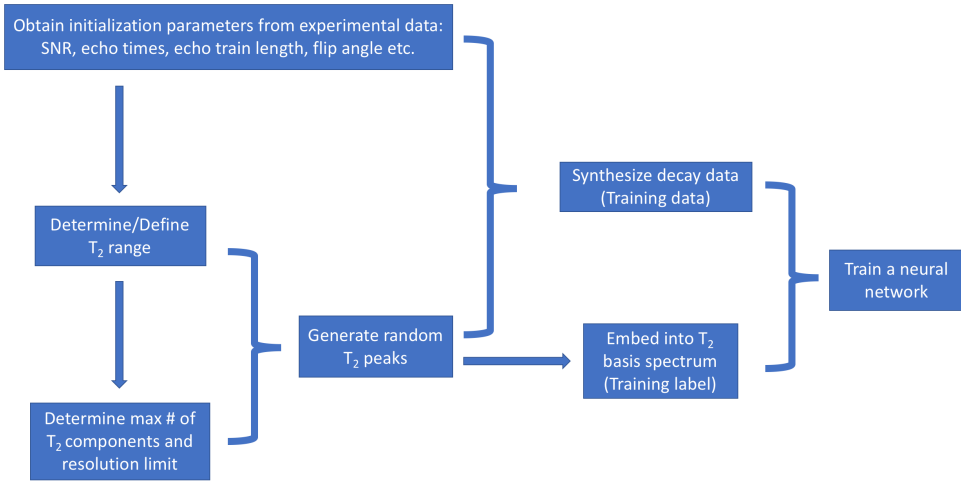


FIGURE 1 SAME-ECOS workflow.

ground truth spectrum labels; (5) apply the trained neural network model to experimental data. In general, SAME-ECOS is a simulation-derived solver, powered by information theory and machine learning, to the problem of fitting multi-exponential decay data into a T_2 spectrum. It is worth highlighting that SAME-ECOS has high flexibility of tailoring itself to different experimental conditions attributed to its unique simulation workflow. The detailed SAME-ECOS algorithm is demonstrated in the Methods part by presenting an example with in-depth explanations.

2 | METHODS

Because the SAME-ECOS analysis method is tailored to different MR experimental conditions, we use one specific example here as a paradigm to demonstrate its simulation workflow, trained model evaluation, and experimental data application. Therefore, the Methods part of this introductory paper to SAME-ECOS is presented in the following sections as a particular experiment.

2.1 | In-vivo MRI experiment

32-echo brain data (gradient and spin echo (GRASE), $TE/\Delta TE/TR=10/10/1000$ ms, refocusing flip angle (FA)= 180° , axial matrix size = 232×186 , acquired resolution = $1 \times 1 \times 5$ mm³ for 20 slices, reconstructed resolution = $1 \times 1 \times 2.5$ mm³ for 40 slices, acquisition time = 14.4 minutes) [18] from one healthy volunteer (male, 57 years old) was collected at a 3T scanner (Philips Achieva) using an 8-channel head coil.

2.2 | SAME-ECOS workflow

(1) **Choose the SNR range to be 70-300.** To initialize the simulation workflow, the SNR of the experimental data needs to be determined first, as calculations of the T_2 range, the resolution limit, and especially the noise simulation, all depend on the SNR. The SNR was initially estimated to be approximately 167 by examining the noise variance of the air

voxels proximate to the skull on the 1st echo image. However, most of today's MRI images acquired by multi-channel coils are reconstructed using parallel imaging [19], which complicates the estimation of SNR. Other factors, such as B1 inhomogeneity, may lead to regional variations in SNR. Therefore, the SNR of experimental data cannot be simply assessed by a single definitive number. To accommodate these hurdles, we empirically assigned the SNR a wide range of 70 to 300, instead of using a single value. This approach allows us to randomly select any SNR within the designated range at each simulation realization, making the resulting simulated data 'all-inclusive' after many realizations.

(2) Define the T_2 range to be 7-2000ms. Intuitively, the shortest detectable T_2 decay component should have its residual signal greater than the noise level at the first measurement. Because the first echo is used later as a normalization factor, the second echo is actually regarded as the first measurement in our analysis. In theory, a minimum of two measurement points would be needed for the purpose of T_2 fitting. That means the residual signal of the shortest T_2 component in our analysis should be higher than the noise level at the third echo. Thus, the lower bound of the T_2 range can thus be obtained using equation 1.

$$T_2^{\min} = -\frac{3rd\ echo\ time}{\ln\left(\frac{1}{SNR}\right)} \quad (1)$$

Given the SNR range of 70 to 300, the lower boundary is calculated to be approximately 7ms. On the other hand, an ideal experimental condition would be monitoring the decay as long as possible until the longest T_2 component decays completely. [20, 21, 22] Then the upper bound for the analyzable T_2 range can be determined using equation 2. [3]

$$T_2^{\max} = -\frac{last\ echo\ time}{\ln\left(\frac{1}{SNR}\right)} \quad (2)$$

However, the ideal experimental condition rarely happens as the decay monitoring time is often compromised to achieve a shorter scanning time for most in-vivo MR experiments including our own (last TE = 320ms). If equation 2 were used with our SNR range of 70 to 300, the longest analyzable T_2 component would be less than 80ms, which is considered to be too short for the analysis of in-vivo brain imaging. Therefore, the upper boundary is manually extended to 2000ms based on the literature T_2 ranges for brain. [1, 2, 7]

(3). Determine the maximum number of resolvable T_2 components to be $M = 5$ and the resolution limit $\delta = 3.098$. For a given SNR and T_2 range, the decay components can only be resolved to a certain resolution limit. Link et al. [12] derived an expression (equation 3) relating T_2^{\min} , T_2^{\max} and SNR, to the M resolvable exponentials.

$$\frac{M}{\ln\left(\frac{T_2^{\max}}{T_2^{\min}}\right)} \times \sinh\left(\frac{\pi^2 \times M}{\ln\left(\frac{T_2^{\max}}{T_2^{\min}}\right)}\right) = \left(\frac{SNR}{M}\right)^2 \quad (3)$$

Derivations and justifications of equation 3 can be found in several publications. [3, 11, 12] Based on these previous theoretical studies, the maximum number of resolvable T_2 components $M = 5$ was obtained by numerically solving equation 3 to the nearest integer for the given SNR and T_2 range. Note that $M = 5$ is the universal integer solution to most SNRs in the range of 70-300 in our case. Then, the T_2 resolution limit $\delta = 3.098$ was determined by equation 4. [3]

$$\delta = \left(\frac{T_2^{\max}}{T_2^{\min}}\right)^{\frac{1}{M}} \quad (4)$$

(4). For each simulation realization:

a. generate random integers $n < M$, $FA \in [90^\circ, 180^\circ]$, and $SNR \in [70, 300]$. Note that the simulation did not include the case of $n = M$ because when $n = M$, there is only one possible configuration for the M T_2 locations within the T_2 range obeying the resolution limit, which would introduce an unwanted bias into the simulated dataset. Also note that the actual FA can deviate substantially from the prescribed FA due to B1 inhomogeneity, so we gave a 90° tolerance to account for the FA variations.

b. generate n randomly located T_2 components within the T_2 range obeying the resolution limit δ . The locations and amplitudes of the n T_2 components were randomly assigned and normalized to one.

c. synthesize 32-echo decay data. The pure decay signal without noise of the n T_2 components (denoted as S_{pure}) were synthesized (equation 5) using the extended phase graph (EPG) algorithm [23, 24] with $T_1 = 2000\text{ms}$ as a default.

$$S_{\text{pure}} = \sum_{i=1}^{i=n} \text{Amplitude}_i \times \text{EPG}(T_{2,i}, \text{selected FA}) \quad (5)$$

To mimic the noise profile of a real MRI image [25], the S_{pure} was first projected into the real and imaginary axes by a random phase factor $\theta \in [0^\circ, 90^\circ]$, followed by adding noises on both axes, and finally producing the magnitude of the noisy signal (equation 6).

$$S_{\text{noisy}} = \sqrt{(S_{\text{pure}} \times \sin \theta + \text{noise}_1)^2 + (S_{\text{pure}} \times \cos \theta + \text{noise}_2)^2} \quad (6)$$

where noise_1 and noise_2 were independently sampled from a Gaussian distribution with its mean = 0 and its variance was determined by equation 7

$$\text{Gaussian noise variance} = \frac{1}{\text{selected SNR} \times \sqrt{\pi/2}} \quad (7)$$

such that the noisy signal S_{noisy} would follow a Rician distribution at the selected SNR level. The synthesized noisy decay data were subsequently normalized to the 1st echo and saved for model training.

d. Embed n T_2 components into a spectrum representation depicted by 40 basis T_2 s. The 40 basis T_2 s ($t_1, t_2, t_3, \dots, t_{40}$) were equally spaced within the T_2 range on a logarithmic scale. The 40 weighting factors of the basis T_2 s were used to represent the spectrum of n T_2 components ($T_{2,1}, T_{2,2}, \dots, T_{2,n}$). Explicitly, each T_2 component was depicted as a Gaussian-shaped peak by the basis T_2 s, with the weighting factor w_i of the i^{th} basis T_2 (t_i) being calculated as

$$w_i = \sum_{j=1}^n \frac{1}{\sqrt{2\pi}} e^{-\frac{1}{2}(t_i - T_{2,j})^2} \quad (8)$$

The embedded T_2 basis representation was normalized to one and recorded as the ground truth spectra for model training.

(5) Train a neural network to map the decay data to its T_2 spectrum. A neural network (hidden layers: $100 \times 500 \times 1000 \times 1000 \times 500$, activation: SeLU [26] (hidden layers) and softmax [27] (output layer), optimizer: Adamax [28], loss: categorical cross-entropy [29]) was constructed using TensorFlow [30] to take 32-echo decay data as input and predict the weighting factors of the 40 basis T_2 s at the output layer. The constructed neural network was trained to map the decay data to its T_2 spectrum. We yielded 3,000,000 simulation realizations (step 4), 90% of which were used for the neural network training. The remaining 10% simulation realizations were used for the validation that determined the

Pre-defined spectra	T ₂ locations (ms)	T ₂ amplitudes (normalized)
Spectrum 1	100	1
Spectrum 2	25, 120	0.3, 0.7
Spectrum 3	15, 80, 50	0.3, 0.5, 0.2
Spectrum 4	10, 60, 300, 1200	0.2, 0.4, 0.3, 0.1

TABLE 1 Four pre-defined ground truth spectra. The T₂ locations of each spectrum are selected obeying the resolution limit. Amplitudes are normalized to one.

stopping criterion for the training process. The training was stopped when the accuracy on the validation set did not improve further. This particular trained neural network is denoted as the SAME-ECOS model hereafter and can be applied to new 32-echo decay data to obtain T₂ spectrum.

2.3 | SAME-ECOS model performance evaluation

The performance of the SAME-ECOS model was evaluated using three designed tests and compared respectively with the results determined by a regularized NNLS solver equipped with stimulated echo correction [24] (analysis program can be requested here: <https://mriresearch.med.ubc.ca/news-projects/myelin-water-fraction/>). The kernel matrix for the NNLS analysis was adjusted accordingly to match our experimental and simulation parameters. The regularization parameter was chosen to be the largest value that allows a misfit of less than 1.02 times of the minimum misfit, which is commonly used in many studies. [31, 32, 33, 34, 35]

Test 1: 300,000 ground truth T₂ spectra and their noisy 32-echo decay data were randomly generated following the workflow described in section 2.2. The decay data were analyzed by the SAME-ECOS model and NNLS respectively to produce the T₂ spectra. The processing time was recorded. The 'goodness' of each spectrum fitting by both methods was quantitatively assessed using cosine similarity scores [36], which report values between 0 to 1, with 0 being the least similar and 1 being the most similar to the ground truth labels. The cosine similarity score is a commonly used metric that measures the similarities between two vectors, especially when the vectors are high dimensional. It is a suitable metric for our task since each T₂ spectrum can be treated as a vector of 40 dimensions. The calculation of the cosine similarity score is defined explicitly in the following formula

$$\text{cosine similarity score} = \frac{X \bullet Y}{\|X\| \times \|Y\|} \quad (9)$$

Where X and Y are the vector representations of the predicted and the ground truth spectra; $\|X\|$ and $\|Y\|$ are their Euclidean norms respectively. Paired t-test was performed to determine whether there was a significant difference ($P < 0.05$) in the cosine similarity scores calculated by SAME-ECOS and NNLS.

Test 2: To examine the model robustness to noise, simulated decay data of 4 pre-defined ground truth T₂ spectra (Table 1) at SNR = 100 and FA = 180°, each with 100 different noise realizations, were passed to the SAME-ECOS model and NNLS for spectrum predictions. The location and amplitude of each ground truth spectrum were manually chosen to provide a visual-friendly data presentation. The spectrum analysis results of both SAME-ECOS and NNLS were normalized (sum to unity) prior to comparison. The similarity between each predicted and ground truth spectrum was assessed by cosine similarity scores defined above. The mean and standard deviation of the cosine similarity scores were also calculated.

Test 3: 10,000 ground truth T_2 spectra and their 32-echo decay data with noise realizations were randomly generated according to steps described in section 2.2. The decay data were analyzed by the SAME-ECOS model and NNLS respectively to produce the T_2 spectra. The myelin water fraction (MWF, a fraction of signal with $T_{2s} < 40\text{ms}$)² was extracted from each predicted spectrum and compared with the ground truth MWF. Mean absolute error (MAE) in the MWF estimation was computed. The correlation between the errors of MWF estimation and the FA was evaluated using Pearson correlation analysis.

2.4 | Apply SAME-ECOS to experimental data

The SAME-ECOS model was applied to the experimental in-vivo GRASE data, which were pre-processed by normalizing to the first echo image. The processing time for the whole brain data analysis was recorded. From the resulting T_2 spectra, the MWF ($T_{2s} < 40\text{ms}$) was extracted for each voxel. The masks of regions of interest (ROI) including whole brain, whole white matter, corpus callosum, corticospinal tract, forceps major, and forceps minor were produced using the first echo image via the FSL segmentation tool. [37] The T_2 spectra and MWF map was also produced using NNLS in the T_2 range of 7-2000ms as a reference for comparison.

3 | RESULTS

3.1 | Performance evaluation via simulation tests

3.1.1 | Test 1: general performance

The processing time to make 300,000 spectra predictions was 22 seconds for the SAME-ECOS model and 1,620 seconds for NNLS (CPU: Intel(R) Core(TM) i7-5930K @ 3.5 GHz, 32 GB RAM). The mean cosine similarity score of the 300,000 spectra predicted by the SAME-ECOS model (0.838 ± 0.189) was significantly higher ($p < 0.05$) than that of the NNLS (0.741 ± 0.160).

3.1.2 | Test 2: robustness to noise

The resulting SAME-ECOS and NNLS spectra from each individual noise realization (grey) were plotted in **Figure 2** to compare against the ground truth spectrum (green). The average spectrum from 100 different noise realizations was also calculated for all SAME-ECOS and NNLS scenarios (blue: SAME-ECOS, red: NNLS). SAME-ECOS produced visually better results than NNLS for all scenarios. For spectra consisting of one or two T_2 components, the SAME-ECOS model was able to make almost perfect predictions (cosine similarity score: 0.998 ± 0.002 and 0.951 ± 0.05649 , respectively); NNLS could also make accurate predictions but with more substantial variability (cosine similarity score: $0.913 \pm 0.0.028$ and 0.802 ± 0.093 , respectively). For spectra consisting of three or four T_2 components, the performances of both methods started to degrade. However, SAME-ECOS (cosine similarity score: 0.681 ± 0.154 , 0.579 ± 0.128 , respectively) was still making better predictions than NNLS (cosine similarity score: 0.572 ± 0.127 , 0.573 ± 0.085 , respectively).

3.1.3 | Test 3: MWF prediction accuracy

MWF values were extracted using both SAME-ECOS and NNLS methods and plotted against 10,000 ground truth MWF values in **Figure 3**. SAME-ECOS MWF (blue, MAE=0.050) demonstrated slightly better agreement with the ground

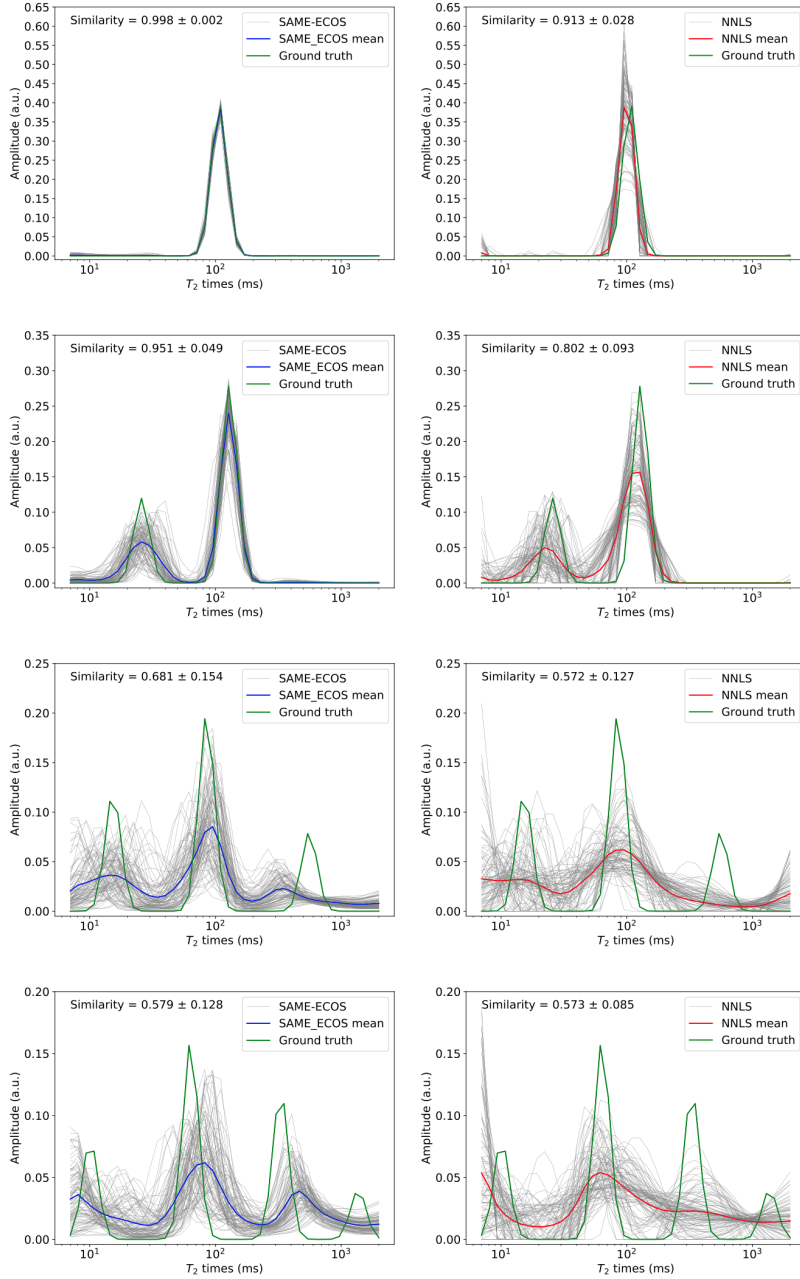


FIGURE 2 T_2 spectra produced by SAME-ECOS (blue) and NNLS (red) respectively are compared with the ground truth spectra (green). Simulated decay data, which are generated from 4 pre-defined ground truth spectra (Table 1) each with 100 different noise realizations, are fed into the trained SAME-ECOS model and NNLS algorithm to generate the T_2 spectra. Faded gray lines indicate the produced spectra for each noise realization. The mean and standard deviation of cosine similarity scores of 100 realizations are shown for each sub-figure.

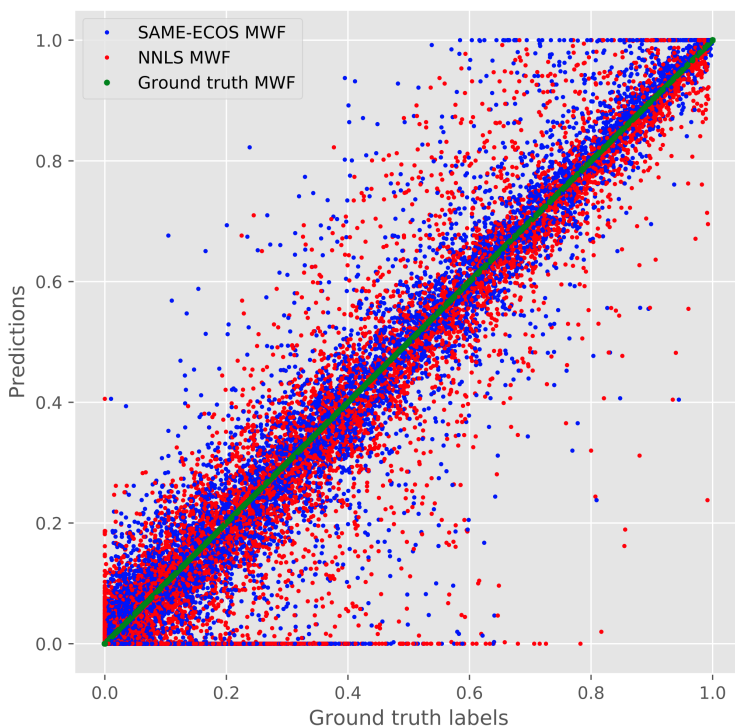


FIGURE 3 Myelin water fraction (MWF) produced by SAME-ECOS (blue) and NNLS (red) are compared with the ground truth MWF (green). 10,000 randomly simulated decay data examples were analyzed by SAME-ECOS and NNLS respectively. The MWF (fraction of signal with $T_{2s} < 40\text{ms}$) was extracted from each predicted spectrum.

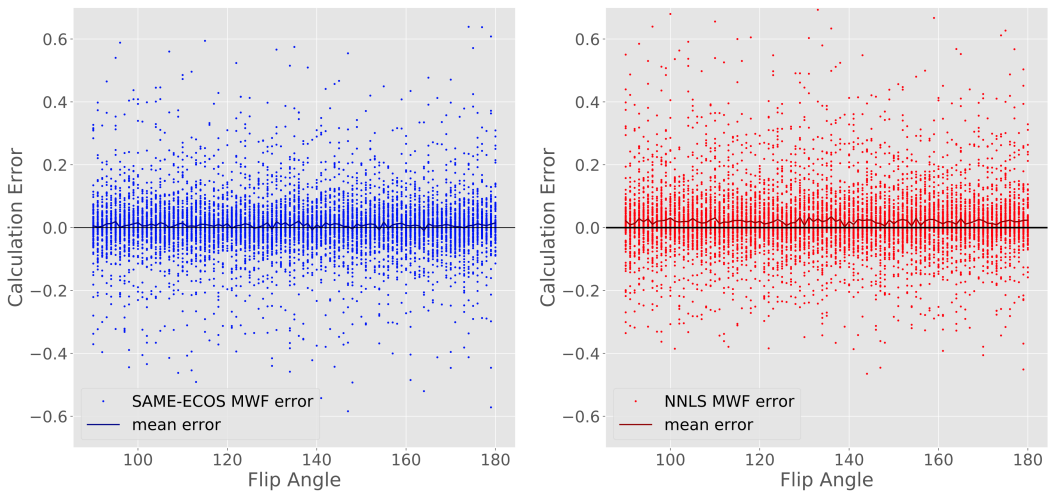


FIGURE 4 Flip angle (FA) dependence of myelin water fraction (MWF) prediction errors. 10,000 randomly simulated decay data examples were analyzed by SAME-ECOS and NNLS. Errors of MWF (fraction of signal with $T_2s < 40ms$) was calculated and compared with FA. The mean error of each FA was also presented for a visual check for biases.

truth (green) than NNLS MWF (red, MAE=0.058). The MWF prediction errors of both methods are plotted against the FA in **Figure 4**, where the mean error of each FA was also presented for a visual check for biases. A small but noticeable positive bias (0.019, overestimation of MWF) was observed for the NNLS method, whereas SAME-ECOS did not show any obvious bias (0.007).

3.2 | In-vivo experimental data: MWF maps

In-vivo GRASE data were analyzed by the SAME-ECOS model and NNLS. The processing times of the whole brain data were 3 minutes for the SAME-ECOS model and 86 minutes for NNLS. Six representative slices of the GRASE first echo, the resulting MWF maps produced by both methods ($T_2s < 40ms$), and the voxel-wise MWF difference map (SAME-ECOS MWF – NNLS MWF), are presented in **Figure 5**. The SAME-ECOS MWF map is visually very similar to the NNLS MWF map, but subtle differences are still visible. Quantitatively, the SAME-ECOS mean MWF of whole white matter (0.131 ± 0.080) is lower than that of the NNLS approach (0.152 ± 0.078). **Figure 6** shows the voxel spectra, the mean spectra, and the mean MWF within the ROIs of the corpus callosum, corticospinal tract, forceps major and forceps minor. The SAME-ECOS mean MWF was lower than the NNLS mean MWF for most ROIs (except for forceps major). It is observed that for all ROIs, the SAME-ECOS mean spectra are able to resolve a short T_2 peak (attributed to myelin water) in addition to a more dominate middle peak (attributed to IE water), whereas the NNLS mean spectra can only resolve a single broad middle peak.

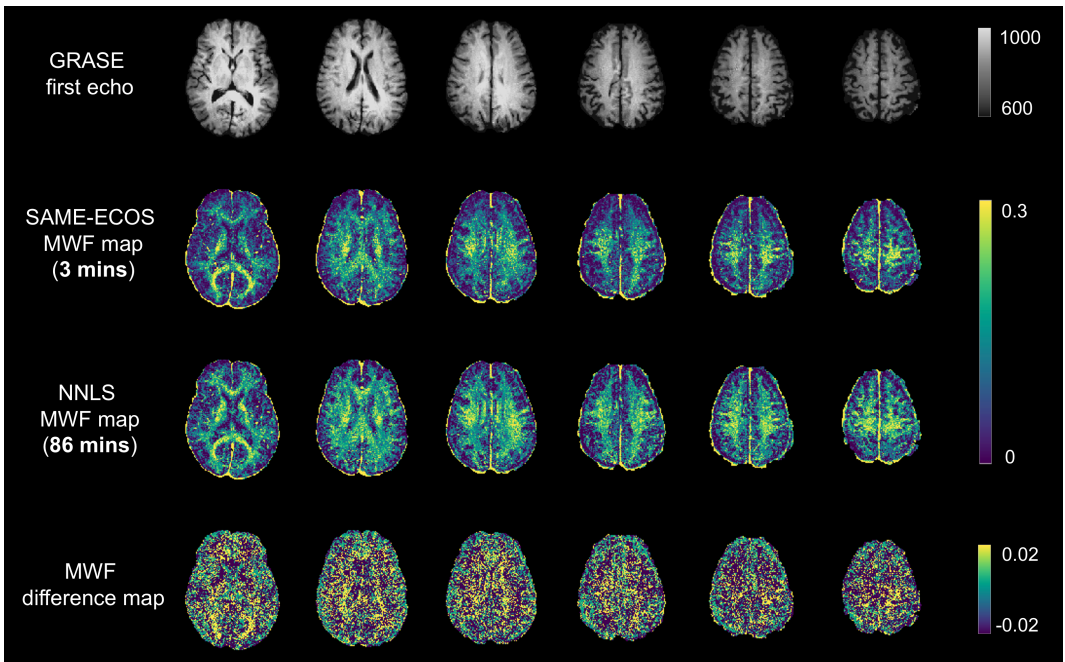


FIGURE 5 SAME-ECOS and NNLS derived in-vivo myelin water fraction maps. Six representative slices of the GRASE first echo, the resulting MWF maps produced by both methods ($T_2s < 40ms$), and the voxel-wise MWF difference map (SAME-ECOS MWF – NNLS MWF), are shown.

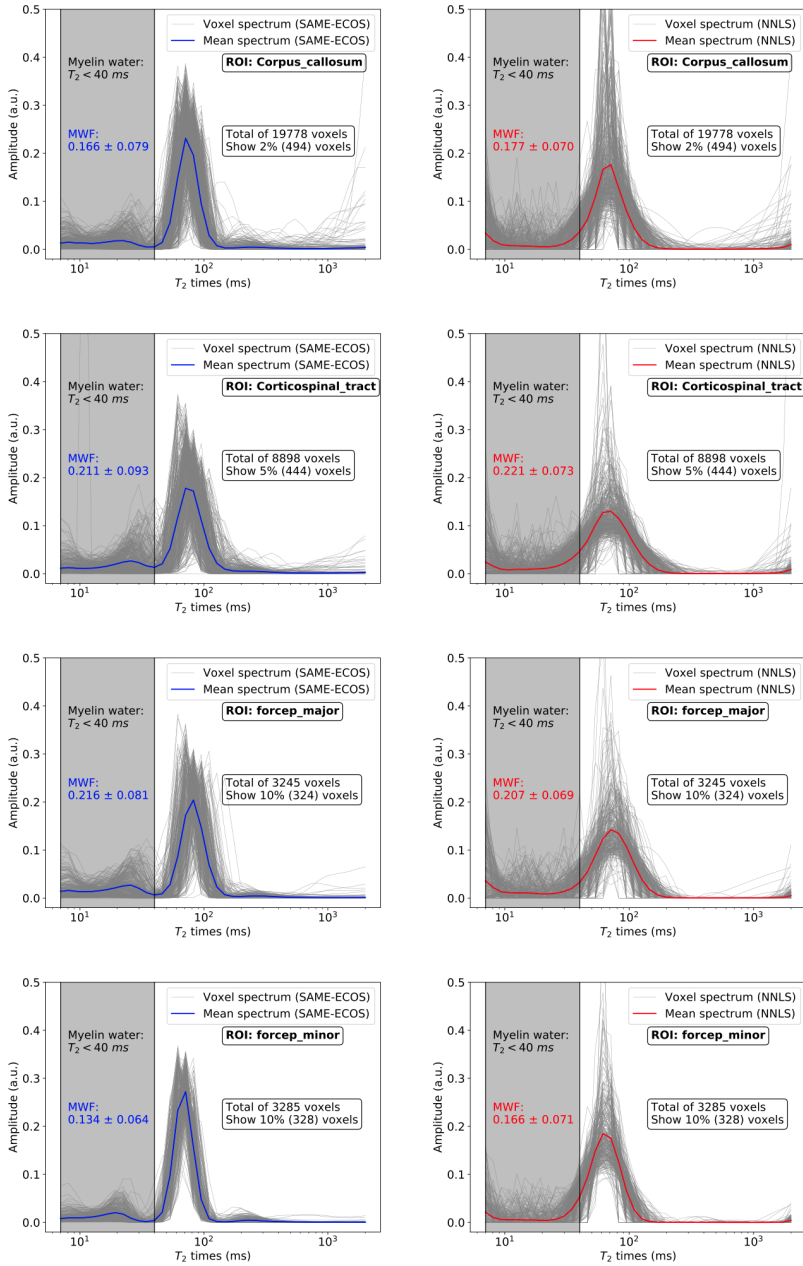


FIGURE 6 Voxel spectra (gray), the mean spectra (blue: SAME-ECOS; red: NNLS), and the mean MWF ($T_2 < 40\text{ms}$) within the four ROIs of the experimental in-vivo data. ROIs include the corpus callosum, corticospinal tract, forceps major, and forceps minor. The voxel spectra are only plotted for a fraction of the total number of voxels for a visual-friendly presentation as indicated in each subfigure. The mean spectrum and mean MWF are calculated from all voxels within each ROI.

4 | DISCUSSION

4.1 | SAME-ECOS vs. NNLS

From the results of all three simulation tests, the SAME-ECOS model largely outperformed NNLS. Using NNLS as the baseline, the SAME-ECOS model achieved 13.1% higher overall cosine similarity scores (**Test 1**), and 16.0% lower MAE of MWF predictions (**Test 3**), as well as demonstrated better robustness to noise (**Test 2**). Specifically, from visual inspection of the results presented in **Figure 2**, both methods were able to produce accurate T_2 spectra when the number of T_2 components $n \leq 2$. However, when $n > 2$, the NNLS predictions became extremely unstable, resulting in over-smoothed mean spectra. This observation illustrates that, unlike NNLS being highly susceptible to noise, the SAME-ECOS model has a desirable feature of being relatively noise-inert. It is also noticed that both methods were incapable of producing reliable spectrum predictions particularly for the long T_2 components (e.g. $T_2s > 500ms$), which is likely due to the relatively short measurement time (the last $TE=320ms$) so there was not enough information acquired to resolve the long T_2 component accurately. In addition, as illustrated in **Figure 4**, NNLS was systematically overestimating MWF throughout the FA range under our investigation. In contrast, SAME-ECOS produced more accurate MWF values without any obvious biases. Overall, the current SAME-ECOS model demonstrated a better performance than NNLS in the interrogations using simulation tests.

Due to the lack of ground truth, it is difficult to judge which method is more accurate when it comes to in-vivo experimental data. However, in terms of data processing speed, SAME-ECOS is approximately 30 times faster than NNLS, achieving a whole-brain analysis in 3 minutes, which is more feasible in clinical settings. From a visual inspection of the MWF maps shown in **Figure 5**, these two methods produced similar results, but the SAME-ECOS MWF map appeared to be a little less noisy, making its white and gray matter distinction slightly more prominent. Interestingly, compared with SAME-ECOS, the NNLS mean MWF values in white matter regions were higher, which coincided with the NNLS MWF overestimation issue presented in **Figure 4**.

A thorough analysis of the NNLS spectra in a few white matter ROIs (**Figure 6**) revealed that the NNLS MWF signal (T_2 cutoff at 40ms) largely originated from the broad middle peak, which is commonly designated as the IE water pool. There was not much contribution from a separate myelin water pool ($T_2s < 40ms$) to the NNLS MWF, and the myelin water peak did not exist on the NNLS mean spectra for all ROIs. In contrast, the myelin water peak and its separation with the IE water peak were easily seen on the SAME-ECOS mean spectra for all ROIs (**Figure 6**), aligning with the intuitive interpretation of MWF arising entirely from a separate myelin water pool. Thus, this observation raises a concern that reporting MWF values alone may not fully unveil the underlying information, especially for those myelin water imaging studies that used NNLS. Nevertheless, future studies using histological validation [38, 39] should be conducted to better compare these two analysis methods in dealing with experimental data.

4.2 | Advantages of SAME-ECOS

The biggest advantage of SAME-ECOS lies in the fact that it is a simulation-derived solver, which takes a fundamentally different route to yield the solutions compared with conventional solvers such as NNLS. Its unique workflow makes SAME-ECOS highly tailorable to different experimental conditions and the needs of analysis. Most parameters used in SAME-ECOS are tunable. For example, the T_1 parameter was set to be a constant for all T_2 components in our simulation because the T_1 weighting is minimized by using GRASE. But if a sequence sensitive to both T_1 and T_2 were used, one could simply turn the T_1 parameter into another variable for the production of training data and make the training labels a 2D map that resolves distinct components with different T_1 , T_2 times. [40] In contrast, it is presumably more difficult

to include either T_1 or any other quantities as an additional variable in the NNLS analysis. Another example would be how easily the influence of B1 inhomogeneity is handled. SAME-ECOS simply treats the refocusing FA as a variable when producing the simulated decay data to account for the FA variations caused by B1 inhomogeneity. However, the same problem was not solved using NNLS for many years until Prasloski et al. [24] proposed to integrate the stimulated echo correction into the original NNLS algorithm, which was a tremendous effort for such integration. Furthermore, if one wants to subject the data analysis to a simpler 3-pool model for instance, SAME-ECOS can easily be simplified to a 3-pool solver by fixing the number of T_2 components to be $n=3$ in the simulation, although it is not encouraged to do so for reasons discussed later. Conclusively, SAME-ECOS is extremely tunable to accommodate either a simpler or more complex model.

Another advantage of SAME-ECOS is to utilize the concept of resolution limit from information theory to prevent overfitting of noise. Due to unavoidable noise contamination, T_2 components can only be recovered to a certain extent, and any violation to the law of resolution limit should be theoretically prohibited. The essential part of SAME-ECOS workflow is to obey the resolution limit to prevent any solutions with adjacent T_2 components being too close together, a feature which is not guaranteed in the solutions of NNLS or any other methods to our knowledge. One reasonable concern that is raised here is that nature does not know about resolution limits, so what happens when adjacent T_2 components really are too close together? Unfortunately, the answer is that we might never resolve these two peaks in a solution where they are bound to degenerate into one peak due to the limited SNR, as Istratov et al. [3] pointed out about this particular problem: "Many physicists have discovered after much wasted effort that it is essential to understand the ill-conditioned nature of the problem before attempting to compute solutions". On the other hand, the commonly used NNLS has incorporated regularization techniques [41] to mitigate the noise overfitting, but the choice of regularization parameters is poorly justified in most of the MR literature. From a technical perspective, the strength of regularization should be selected based on the local SNR rather than being universally fixed. Unfortunately, this has never been practiced in the NNLS analysis due to technical challenges. In addition, the noise of a magnitude MRI image originates from Gaussian distributed noise on both real and imaginary channels [25], which is not accounted for in the NNLS method [42] but is correctly modelled in the SAME-ECOS approach. Particularly in the last few echoes, when there is no residuals of MR signal (only pure noise), the noise profile would follow a Rayleigh distribution on the magnitude image that always has positive values, such that NNLS could misinterpret the Rayleigh noise as a long T_2 component that has not been completely decayed yet. This phenomenon is observed in **Figure 6**, where NNLS mean spectra (red) for all ROIs always give a little rise on the far side of long T_2 s ($T_2 = 2000$ ms), but SAME-ECOS mean spectra (blue) is free of this problem.

SAME-ECOS also takes advantage of the strong predictive power of a fine-tuned neural network. For regression problems such as our T_2 -fitting task, modern machine learning methods like neural networks usually outperform conventional statistical methods in terms of better prediction accuracy and faster data processing speed [17], which is exactly what we have observed in our simulation tests. Out of various machine learning methods, the neural network approach is favored for use in the current SAME-ECOS workflow because it has been successfully implemented in similar tasks by different research groups. [15, 16, 43] In theory, other machine learning methods may also achieve a similar predictive power. Comparisons between different machine learning methods are beyond the scope of this paper, but could be an area of future investigation.

Finally, it is worth highlighting that the simulated training dataset of SAME-ECOS is not informed by any prior knowledge (e.g. a 2-pool model is informed by the T_2 times of myelin water and IE water, or a typical range of the MWF values obtained from previous studies). Instead, SAME-ECOS is completely driven by a large number of random simulations, which are only regulated by the experimental conditions such as SNR. This approach should be valued and favored because it is absolutely immune to (1) the potential errors of previous findings where the prior information

is acquired from; (2) the biases that prior information may introduce into the analysis results. Simply speaking, an informed model is more likely to perform the analysis with a bias naturally towards the prior information. Similar to NNLS, no prior information being needed is a desirable and specially designed feature of SAME-ECOS.

4.3 | Disadvantages of SAME-ECOS

A major concern of SAME-ECOS is that its fitting results are not easily verified mathematically due to the use of a neural network. SAME-ECOS is capable of producing reliable results only on data that are similarly distributed as the training data. SAME-ECOS may become unpredictable and yield uninterpretable results when applied to unfamiliar data. Although we have generated a large training dataset by the simulations to account for many types of variations, there is no doubt that real experimental data have far more complexity in them. Factors such as artifacts are detrimental to any analysis methods, but SAME-ECOS is potentially less predictable. Unlike SAME-ECOS which empirically analyzes the data, conventional methods process the data either analytically or numerically, making them somewhat more mathematically explainable and predictable when encountering these problems.

Another limitation of SAME-ECOS is related to standardization. The variety of parameters such as the T_2 range, the noise profiles, the number of neural network hidden layers etc. can be manually selected at the user's will, which offers flexibility and customizability, but it is difficult to propose a standard SAME-ECOS model that works universally. The effects of changing these parameters warrants further investigation. Although SAME-ECOS demonstrated excellent performance in our simulation tests and in-vivo example application, users should further validate SAME-ECOS on their own experimental data before replacing any conventional analysis methods.

4.4 | Other quantitative MRI techniques and beyond

Within MRI, the usage of SAME-ECOS is not just limited to multi-echo relaxation sequences. As long as the spins are trackable by simulations, then the SAME-ECOS methodology should also be applicable to other quantitative MRI techniques, such as multi-component driven equilibrium single pulse observation of T_1 and T_2 (mcDESPOT) [44] and neurite orientation dispersion and density imaging (NODDI) [45], by modifying the current workflow accordingly. Beyond MRI, it is also possible to apply SAME-ECOS to any quantitative sciences that involve multi-exponential decays. In general, we believe a simulation-derived solver like SAME-ECOS is an alternative way to produce at least comparable results to conventional methods. It may deliver better performance, especially when analytical and numerical solutions start to fail due to factors such as a limited amount of data points and low SNR. Nevertheless, the SAME-ECOS methodology seems to have the potential to be generalized for the analysis of decay data within and beyond the MRI field.

5 | CONCLUSION

We have introduced a novel method SAME-ECOS, which can decompose multi-exponential MR relaxation data into a T_2 spectrum. SAME-ECOS is highly tailorable to different experimental conditions and various analysis models. Compared with the commonly used method NNLS, our results have demonstrated that SAME-ECOS can yield much more reliable T_2 spectra and MWF values in a dramatically shorter processing time, by utilizing information theory and machine learning simultaneously.

ACKNOWLEDGEMENTS

We thank the study participants and the excellent MRI technologists at UBC MRI Research Center. Funding support was provided by the Multiple Sclerosis Society of Canada, Natural Sciences and Engineering Research Council Discovery Grant.

REFERENCES

- [1] Whittall KP, MacKay AL, Li DK. Are mono-exponential fits to a few echoes sufficient to determine T2 relaxation for in vivo human brain? *Magnetic Resonance in Medicine: An Official Journal of the International Society for Magnetic Resonance in Medicine* 1999;41(6):1255–1257.
- [2] Mackay A, Whittall K, Adler J, Li D, Paty D, Graeb D. In vivo visualization of myelin water in brain by magnetic resonance. *Magnetic resonance in medicine* 1994;31(6):673–677.
- [3] Istratov AA, Vyvenko OF. Exponential analysis in physical phenomena. *Review of Scientific Instruments* 1999;70(2):1233–1257.
- [4] Whittall KP, MacKay AL. Quantitative interpretation of NMR relaxation data. *Journal of Magnetic Resonance (1969)* 1989;84(1):134–152.
- [5] Lawson CL, Hanson RJ. Solving least squares problems. SIAM; 1995.
- [6] Provencher SW. CONTIN: a general purpose constrained regularization program for inverting noisy linear algebraic and integral equations. *Computer Physics Communications* 1982;27(3):229–242.
- [7] Kroeker RM, Henkelman RM. Analysis of biological NMR relaxation data with continuous distributions of relaxation times. *Journal of Magnetic Resonance (1969)* 1986;69(2):218–235.
- [8] Du YP, Chu R, Hwang D, Brown MS, Kleinschmidt-DeMasters BK, Singel D, et al. Fast multislice mapping of the myelin water fraction using multicompartiment analysis of T decay at 3T: A preliminary postmortem study. *Magnetic Resonance in Medicine: An Official Journal of the International Society for Magnetic Resonance in Medicine* 2007;58(5):865–870.
- [9] Akhondi-Asl A, Afacan O, Mulkern RV, Warfield SK. T2-Relaxometry for Myelin Water Fraction Extraction Using Wald Distribution and Extended Phase Graph. In: *International Conference on Medical Image Computing and Computer-Assisted Intervention Springer*; 2014. p. 145–152.
- [10] Bertero M, Boccacci P, Pike ER. On the recovery and resolution of exponential relaxation rates from experimental data: a singular-value analysis of the Laplace transform inversion in the presence of noise. *Proceedings of the Royal Society of London A Mathematical and Physical Sciences* 1982;383(1784):15–29.
- [11] McWhirter J, Pike ER. On the numerical inversion of the Laplace transform and similar Fredholm integral equations of the first kind. *Journal of Physics A: Mathematical and General* 1978;11(9):1729.
- [12] Link N, Bauer S, Ploss B. Analysis of signals from superposed relaxation processes. *Journal of applied physics* 1991;69(5):2759–2767.
- [13] Schmidhuber J. Deep learning in neural networks: An overview. *Neural networks* 2015;61:85–117.
- [14] Lundervold AS, Lundervold A. An overview of deep learning in medical imaging focusing on MRI. *Zeitschrift für Medizinische Physik* 2019;29(2):102–127.
- [15] Cohen O, Zhu B, Rosen MS. MR fingerprinting deep reconstruction network (DRONE). *Magnetic resonance in medicine* 2018;80(3):885–894.

- [16] Liu H, Xiang QS, Tam R, Dvorak AV, MacKay AL, Kolind SH, et al. Myelin water imaging data analysis in less than one minute. *NeuroImage* 2020;210:116551.
- [17] Hornik K, Stinchcombe M, White H, et al. Multilayer feedforward networks are universal approximators. *Neural networks* 1989;2(5):359–366.
- [18] Prasloski T, Rauscher A, MacKay AL, Hodgson M, Vavasour IM, Laule C, et al. Rapid whole cerebrum myelin water imaging using a 3D GRASE sequence. *Neuroimage* 2012;63(1):533–539.
- [19] Deshmane A, Gulani V, Griswold MA, Seiberlich N. Parallel MR imaging. *Journal of Magnetic Resonance Imaging* 2012;36(1):55–72.
- [20] Shapiro FR, Senturia SD, Adler D. The use of linear predictive modeling for the analysis of transients from experiments on semiconductor defects. *Journal of applied physics* 1984;55(10):3453–3459.
- [21] Dobaczewski L, Kaczor P, Hawkins I, Peaker A. Laplace transform deep-level transient spectroscopic studies of defects in semiconductors. *Journal of applied physics* 1994;76(1):194–198.
- [22] Thomasson W, Clark Jr J. Analysis of exponential decay curves: A three-step scheme for computing exponents. *Mathematical Biosciences* 1974;22:179–195.
- [23] Hennig J. Multiecho imaging sequences with low refocusing flip angles. *Journal of Magnetic Resonance (1969)* 1988;78(3):397–407.
- [24] Prasloski T, Mädler B, Xiang QS, MacKay A, Jones C. Applications of stimulated echo correction to multicomponent T2 analysis. *Magnetic resonance in medicine* 2012;67(6):1803–1814.
- [25] Cárdenas-Blanco A, Tejos C, Irrarrazaval P, Cameron I. Noise in magnitude magnetic resonance images. *Concepts in Magnetic Resonance Part A: An Educational Journal* 2008;32(6):409–416.
- [26] Klambauer G, Unterthiner T, Mayr A, Hochreiter S. Self-normalizing neural networks. In: *Advances in neural information processing systems*; 2017. p. 971–980.
- [27] Bishop CM. *Pattern recognition and machine learning*. springer; 2006.
- [28] Kingma DP, Ba J. Adam: A method for stochastic optimization. *arXiv preprint arXiv:1412.6980* 2014;.
- [29] LeCun Y, Bengio Y, Hinton G. Deep learning. *nature* 2015;521(7553):436–444.
- [30] Abadi M, Agarwal A, Barham P, Brevdo E, Chen Z, Citro C, et al. Tensorflow: Large-scale machine learning on heterogeneous distributed systems. *arXiv preprint arXiv:1603.04467* 2016;.
- [31] Dvorak AV, Ljungberg E, Vavasour IM, Liu H, Johnson P, Rauscher A, et al. Rapid myelin water imaging for the assessment of cervical spinal cord myelin damage. *NeuroImage: Clinical* 2019;23:101896.
- [32] Liu H, Rubino C, Dvorak AV, Jarrett M, Ljungberg E, Vavasour IM, et al. Myelin water atlas: a template for myelin distribution in the brain. *Journal of Neuroimaging* 2019;29(6):699–706.
- [33] Liu H, Ljungberg E, Dvorak AV, Lee LE, Yik JT, MacMillan EL, et al. Myelin water fraction and intra/extracellular water geometric mean T2 normative atlases for the cervical spinal cord from 3T MRI. *Journal of Neuroimaging* 2020;30(1):50–57.
- [34] Lee LE, Ljungberg E, Shin D, Figley CR, Vavasour IM, Rauscher A, et al. Inter-vendor reproducibility of myelin water imaging using a 3D gradient and spin echo sequence. *Frontiers in Neuroscience* 2018;12:854.
- [35] Ljungberg E, Vavasour I, Tam R, Yoo Y, Rauscher A, Li DK, et al. Rapid myelin water imaging in human cervical spinal cord. *Magnetic resonance in medicine* 2017;78(4):1482–1487.

- [36] Han J, Pei J, Kamber M. *Data mining: concepts and techniques*. Elsevier; 2011.
- [37] Zhang Y, Brady M, Smith S. Segmentation of brain MR images through a hidden Markov random field model and the expectation-maximization algorithm. *IEEE transactions on medical imaging* 2001;20(1):45–57.
- [38] Laule C, Kozlowski P, Leung E, Li DK, MacKay AL, Moore GW. Myelin water imaging of multiple sclerosis at 7 T: correlations with histopathology. *Neuroimage* 2008;40(4):1575–1580.
- [39] Laule C, Leung E, Li DK, Traboulsee A, Paty D, MacKay A, et al. Myelin water imaging in multiple sclerosis: quantitative correlations with histopathology. *Multiple Sclerosis Journal* 2006;12(6):747–753.
- [40] Celik H, Bouhrara M, Reiter DA, Fishbein KW, Spencer RG. Stabilization of the inverse Laplace transform of multiexponential decay through introduction of a second dimension. *Journal of Magnetic Resonance* 2013;236:134–139.
- [41] Tihonov AN. Solution of incorrectly formulated problems and the regularization method. *Soviet Math* 1963;4:1035–1038.
- [42] Bjarnason TA, McCreary CR, Dunn JF, Mitchell JR. Quantitative T2 analysis: the effects of noise, regularization, and multivoxel approaches. *Magnetic Resonance in Medicine: An Official Journal of the International Society for Magnetic Resonance in Medicine* 2010;63(1):212–217.
- [43] Lee J, Lee D, Choi JY, Shin D, Shin HG, Lee J. Artificial neural network for myelin water imaging. *Magnetic Resonance in Medicine* 2020;83(5):1875–1883.
- [44] Deoni SC, Rutt BK, Arun T, Pierpaoli C, Jones DK. Gleaning multicomponent T1 and T2 information from steady-state imaging data. *Magnetic Resonance in Medicine: An Official Journal of the International Society for Magnetic Resonance in Medicine* 2008;60(6):1372–1387.
- [45] Zhang H, Schneider T, Wheeler-Kingshott CA, Alexander DC. NODDI: practical in vivo neurite orientation dispersion and density imaging of the human brain. *Neuroimage* 2012;61(4):1000–1016.